Analytic Continuum Forward Kinematics of Deformable Linear Objects under Static Conditions

Andreas Müller

***Abstract*—Elastic rods are key functional elements in continuum robots, but also represent elastic objects to be manipulated by robotic manipulators. Such objects are modeled as Cosserat-Reissner rods, and more frequently as Kirchhoff rods exhibiting large deformations but linear material constitutive relations, regarded as deformable linear objects (DLO). Control of continuum robots and robotic manipulation planning rest on a realistic modeling and representation of the shape of a rod from the limited information available. In this note, a computationally efficient and robust algorithm is described that admits to determine a closed form analytic description of the shape of a Kirchhoff rod solely from the knowledge of the orientation and position of its terminal ends. The latter is available from the pose of the robot end-effector in case of robotic manipulation of DLO. The shape is represented as a curve in $SE(3)$.**

***Index Terms*—Continuum robot, deformable linearly object, Cosserat, Kirchhoff, manipulation, forward kinematics, SE(3)**

I. Problem Statement

For navigation of continuum robots, as well as for manipulation planning in context of robotic handling of deformable linear objects (DLO), specifically elastic slender rods, in confined spaces, it is crucial to deduce a reliable estimate of the DLO shape from the relative pose of the terminal ends (or intermediate frames in case of multi-segment continuum robots). This leads to a *continuum forward kinematics (CFK) problem*: Given the end-effector (EE) pose of two robots, $\mathbf{H}_0, \mathbf{H}_1 \in SE(3)$, i.e. the configuration of the DLO's terminal ends, find the curve $\gamma : [0,1] \to SE(3)$ representing the shape of the DLO. Ideally the curve is given in closed form.

II. Prior Work

Elastic rods are modeled with the well established Cosserat theory [1] to capture the spatial deformation of DLO. Its application to the manipulation of DLO and continuum (serial and parallel) robots was put forth in [2], [3], [4]. It is particularly relevant for modeling continuum robots with tubes [5], [6] and soft structures consisting of multiple segments [7]. In many applications, When handling DLO in particular, but in many other situations, shear and compression of the elastic elements are negligible. Restricting the Cosserat model accordingly leads a Kirchhoff rod. The latter were used in [8], for example, to model planar parallel continuum robots and to solve the forward kinematics problem. Kirchhoff rods are deemed more relevant for a majority of applications.

The principal challenge when using Cosserat or Kirchhoff rod theory is the numerical solution of the corresponding boundary value problem [9], [10]. In case of DLO the CFK problem, as stated above, requires solving the governing differential equations for given position and orientation of the terminal ends of a rod. A collocation method is applied in [11] to solve the boundary value problem for Kirchhoff rod. It should be mentioned that also discrete lumped parameter models [12], [13], and closed form solutions of the Euler rod equations for planar deformations [14] were used to enable dual-arm manipulation and shape control.

III. Kinematics of Kirchhoff Rod

A. Geometrically Exact Representation

A Kirchhoff rod (KR) is derived from a Cosserat-Reissner rod (CR) by restricting its deformations to spatial bending ad torsion. A CR is a curve in $SE(3)$ that describes the displacement of a frame $\mathcal{F}_\tau$ (located at the rod's center line, which is aligned with its x-axis) attached at the cross section relative to a frame $\mathcal{F}_0$ attached at the start of the rod. This relative frame motions is represented by $\mathbf{H}(\tau) = \left[\begin{smallmatrix} \mathbf{R}(\tau) & \mathbf{r}(\tau) \\ \mathbf{0} & 1 \end{smallmatrix}\right] \in SE(3)$, with normalized parameter $\tau \in [0,1]$. At the terminal end, frame $\mathcal{F}_1$ is attached. The cross section displacement at start and end of the rod are $\mathbf{H}_0 := \mathbf{H}(0)$ and $\mathbf{H}_1 := \mathbf{H}(1)$, and the relative configuration of the start and terminal ends is $\mathbf{H}_{01} = \mathbf{H}_0^{-1}\mathbf{H}_1 = \left[\begin{smallmatrix} \mathbf{R}_{01} & \mathbf{r}_{01} \\ \mathbf{0} & 1 \end{smallmatrix}\right]$. The deformation screw, represented in $\mathcal{F}_\tau$, is described by $\boldsymbol{\chi} = \left[\begin{smallmatrix} \boldsymbol{\kappa} \\ \boldsymbol{\rho} \end{smallmatrix}\right] \in \mathbb{R}^6$, where κ_1 is the torsion, κ_2, κ_3 the two bending curvatures, ρ_1 is the compression, and ρ_2, ρ_3 are the shear components. The deformation satisfies the Poisson-Darboux equation

$$\hat{\boldsymbol{\chi}} = \mathbf{H}^{-1}\mathbf{H}' \in se(3) \tag{1}$$

or written separately, $\tilde{\boldsymbol{\kappa}} = \mathbf{R}^T\mathbf{R}' \in so(3)$ and $\boldsymbol{\rho} = \mathbf{R}^T\mathbf{r}'$. The strain measure is defined as $\boldsymbol{\chi}(\tau) - \bar{\boldsymbol{\chi}}(\tau)$. Here, $\bar{\boldsymbol{\chi}}$ describes the undeformed rod geometry. If the undeformed rod is straight, then $\bar{\boldsymbol{\chi}} = \left[\begin{smallmatrix} \mathbf{0} \\ \mathbf{e}_1 \end{smallmatrix}\right]$, with $\mathbf{e}_1 = [1\ 0\ 0]^T$. The displacement field, as solution of (1), is expressed with canonical coordinates $\mathbf{X}(\tau) = \left[\begin{smallmatrix} \mathbf{x}(\tau) \\ \mathbf{y}(\tau) \end{smallmatrix}\right] \in \mathbb{R}^6$ as $\mathbf{H}(\tau) = \mathbf{H}_0 \exp \mathbf{X}(\tau)$, with exponential map on $SE(3)$ [15], [16].

A KR does not exhibit shear or compression. With its center line aligned with the x-axis of the cross section frame, for an initially undeformed straight rod, $\boldsymbol{\rho} = \mathbf{e}_1$. Equations (1) yield

$$\mathbf{x}'(\tau) = \mathbf{dexp}^{-1}_{-\mathbf{x}(\tau)} \boldsymbol{\kappa}(\tau) \tag{2}$$

$$\mathbf{r}'(\tau) = \exp \mathbf{x}(\tau)\, \mathbf{e}_1 \tag{3}$$

where $\mathbf{dexp}_{-\mathbf{x}}$ is the matrix form of the right-trivialized differential on $SO(3)$ [16]. While the displacement field of a CR is a curve in $SE(3)$, the displacements of a KR, i.e. solutions of (2) and (3), evolve on a $SE(3)$ submanifold, defined by the constraint $\boldsymbol{\rho} = \mathbf{e}_1$.

B. Analytic Reduced-Order Kinematics

Solutions of (2) describe the angular displacement when the deformation field $\boldsymbol{\kappa}(\tau)$ is given. It was shown [17], [18] that a 3rd-order approximation of the solution curve between initial $\mathbf{R}_0 \in SO(3)$ and terminal orientation $\mathbf{R}_1 \in SO(3)$ is $\mathbf{R}(\tau) = \mathbf{R}_0 \exp \mathbf{x}^{[3]}(\tau)$, with

$$\begin{aligned} \mathbf{x}^{[3]}(\tau) = {} & \left(3\tau^2 - 2\tau^3\right)\bar{\mathbf{x}} + \tau(\tau-1)^2 \boldsymbol{\kappa}_0 \\ & + \left(\tau^3 - \tau^2\right) \mathbf{dexp}^{-1}_{-\bar{\mathbf{x}}} \boldsymbol{\kappa}_1 \end{aligned} \tag{4}$$

[1]Institute of Robotics, Johannes Kepler University Linz, Linz, Austria a.mueller@jku.at

where $\bar{\mathbf{x}} := \log(\mathbf{R}_{01}) \in so(3)$ is the Rodrigues vector defining the relative rotation $\mathbf{R}_{01} = \mathbf{R}_0^T \mathbf{R}_1$, and $\boldsymbol{\kappa}_0 := \boldsymbol{\kappa}(0)$, $\boldsymbol{\kappa}_1 := \boldsymbol{\kappa}(1)$ are boundary values.

A Gauß-Legendre quadrature of order s is used to compute the translation displacement from the orientation field as

$$\mathbf{r}^{[3]}(\tau) = \frac{\tau}{2} \sum_{i=1}^{s} \alpha_i \exp \mathbf{x}^{[3]}(\bar{\tau}_i)\, \mathbf{e}_1. \tag{5}$$

The evaluation points $\bar{\tau}_i := \frac{1}{2}(1+\tau_i)\tau$ are computed from the Gauß points τ_i, and Legendre weights α_i.

IV. Static Equilibria of Kirchhoff Rod

Assuming linear elastic Hookean material, the cross section stiffness matrix $\mathbf{K}_\kappa = \mathrm{diag}(GJ_x, EI_{yy}, EI_{zz})$ is introduced (Young's modulus E, shear stiffness G, cross section area A, second area moments I_{xx}, I_{zz}, polar moment J_x). Then the stress is $\mathbf{K}_\kappa(\boldsymbol{\kappa} - \bar{\boldsymbol{\kappa}})$, and the elastic potential related to the cross section is $\bar{V}_\kappa(\boldsymbol{\kappa}(\tau)) = \frac{1}{2}(\boldsymbol{\kappa}(\tau) - \bar{\boldsymbol{\kappa}}(\tau))^T \mathbf{K}_\kappa(\tau)(\boldsymbol{\kappa}(\tau) - \bar{\boldsymbol{\kappa}}(\tau))$. The overall elastic potential due to bending and torsion is $V_\kappa = \int_0^1 \bar{V}_\kappa(\boldsymbol{\kappa}(\tau))\,\mathrm{d}\tau$. In the absence of external distributed loads, the angular deformation field $\boldsymbol{\kappa}(\tau)$ of a KR in static equilibrium (stationary elastic potential) is the solution of the ODE system

$$\mathbf{K}_\kappa(\boldsymbol{\kappa}' - \bar{\boldsymbol{\kappa}}') + \mathbf{K}_\kappa'(\boldsymbol{\kappa} - \bar{\boldsymbol{\kappa}}) + \tilde{\boldsymbol{\kappa}}\mathbf{K}_\kappa(\boldsymbol{\kappa} - \bar{\boldsymbol{\kappa}}) + \tilde{\mathbf{e}}_1\mathbf{f} = \mathbf{0} \tag{6}$$

where $\tilde{\boldsymbol{\kappa}} \in so(3)$ is the skew symmetric matrix associated to vector $\boldsymbol{\kappa} \in \mathbb{R}^3$, and $\mathbf{f}$ is the constraint force due to the geometric condition $\boldsymbol{\rho} = \mathbf{e}_1$. The solution depends on the initial/boundary values for $\boldsymbol{\kappa}$ and on the constraint force $\mathbf{f}$.

V. Approximate Quasistatic Forward Kinematics

A. Restating the Problem

The quasistatic CFK problem can now be restated: Given initial and terminal orientation and position, $\mathbf{R}_0, \mathbf{r}_0$ and $\mathbf{R}_1, \mathbf{r}_1$, find $\boldsymbol{\kappa}(\tau)$, and the corresponding displacement field such that the elastic potential is minimized. To this end, the potential could be evaluated with the approximate solution (4) and minimized numerically. This computationally simple method yields an analytic expression for the approximate KR shape. The 3rd-order approximation gives rise to yet more efficient method, assuming the elastic potential is minimized if the boundary strains are minimized in a static equilibrium. This assumption is valid for small curvature variations.

The boundary deformations are summarized in the vector $\mathbf{k} := [\boldsymbol{\kappa}_0 \;\; \boldsymbol{\kappa}_1] \in \mathbb{R}^6$. Denote with $||\mathbf{k}||^2_{\mathbf{K}_\mathrm{k}} = \mathbf{k}^T\mathbf{K}_\mathrm{k}\mathbf{k}$ the $\mathbf{K}_\mathrm{k}$-weighted norm of $\mathbf{k}$, where $\mathbf{K}_\mathrm{k} := \left[\begin{smallmatrix}\mathbf{K}_\kappa & \mathbf{0}\\ \mathbf{0} & \mathbf{K}_\kappa\end{smallmatrix}\right]$. The elastic potential associated to the boundary deformations is $\frac{1}{2}||\mathbf{k}||^2_{\mathbf{K}_\mathrm{k}}$, where $\bar{\boldsymbol{\kappa}} = \mathbf{0}$ is assumed (straight undeformed rod). With the above assumption, the problem reduces to find $\boldsymbol{\kappa}_0, \boldsymbol{\kappa}_1$ that minimize $|\mathbf{k}||^2_{\mathbf{K}_\mathrm{k}}$, and using the 3rd-order approximation (4), yields a curve satisfies the geometric terminal conditions. The terminal conditions on the orientation, $\mathbf{R}_0, \mathbf{R}_1$, are satisfied by definition of (4). However, the terminal position $\mathbf{r}_1$ must be imposed as a constraint. The corresponding geometric constraints is $\mathbf{g}(\mathbf{k}) = \mathbf{0}$, with

$$\mathbf{g}(\mathbf{k}) := \mathbf{r}^{[3]}(1) - \mathbf{r}_{01} \tag{7}$$

and the terminal position $\mathbf{r}^{[3]}(1)$ evaluated with (5).

B. Iterative Solution Algorithm

The constraint equations (7) are linearized at a general $\mathbf{k}^*$ as

$$\mathbf{g}(\mathbf{k}^*) + \mathbf{J}(\mathbf{k}^*)\,\mathrm{d}\mathbf{k} = \mathbf{0} \tag{8}$$

where $\mathbf{J}(\mathbf{k}) := \left[\frac{\partial \mathbf{g}(\mathbf{k})}{\partial \boldsymbol{\kappa}_0} \;\; \frac{\partial \mathbf{g}(\mathbf{k})}{\partial \boldsymbol{\kappa}_1}\right]$ is the 3×6 constraint Jacobian. The unique solution minimizing the norm $\|\mathrm{d}\mathbf{k}\|^2_{\mathbf{K}_\mathrm{k}}$ of the change in boundary deformations is $\mathrm{d}\mathbf{k} = -\mathbf{J}^+_{\mathbf{K}_\mathrm{k}}(\mathbf{k})\mathbf{g}(\mathbf{k})$, where $\mathbf{J}^+_{\mathbf{K}_\mathrm{k}} = \mathbf{K}_\mathrm{k}^{-1}\mathbf{J}^T\left(\mathbf{J}\mathbf{K}_\mathrm{k}^{-1}\mathbf{J}^T\right)^{-1}$ is the $\mathbf{K}_\mathrm{k}$-weighted pseudoinverse of $\mathbf{J}$. This gives rise to the following Newton-Raphson iteration scheme (the iteration step is indicated by the superscript i in $\mathbf{k}^i$):

CFK Newton-Raphson Algorithm for Kirchhoff Rods:

Input: $\bar{\mathbf{x}} = \log \mathbf{R}_{01}$ (relative rotation of terminal frames)
$\mathbf{r}_{01}$ (relative translation of terminal frames)

Initialization: $\mathbf{k}^0 := \mathbf{0},\ i := 1$

Do $\mathbf{k}^i := -\mathbf{J}^+_{\mathbf{K}_\mathrm{k}}(\mathbf{k}^{i-1})\mathbf{g}(\mathbf{k}^{i-1})$
$\mathbf{k}^i := \mathbf{k}^{i-1} + \Delta\mathbf{k}^i$
$i := i + 1$

While $\left\|\Delta\mathbf{k}^i\right\| \leq \varepsilon_1 \vee \left\|\mathbf{g}\left(\mathbf{k}^i\right)\right\| \leq \varepsilon_2$

The algorithm terminates when the geometric constraints are satisfied with accuracy ε_2 or when the change in $\mathbf{k}$ is less then specified by ε_1. The initial value $\mathbf{k}^0 = \mathbf{0}$ ensures minimization of the total elastic potential. Another minimum norm solution can be used as start value if available. Due to the use of the 3rd-order approximation, this iteration scheme shows very good robustness and efficiency. It is remarked that the constraint Jacobian can be expressed in closed form making use of analytic relations of the exponential map and derivatives [16].

VI. Examples

The shape reconstruction of a clamped fiberglass rod is used as example. In its undeformed configuration, the rod is straight. The rod has a length $L = 0.6\,\mathrm{m}$, and a constant circular cross section with 2 mm diameter. The elastic material parameters are taken from the manufacturer datasheet. The Young's modulus is $E = 35\,\mathrm{GPa}$, and the shear modulus is $G = 3\,\mathrm{GPa}$. To validate the results, the kinetostatic equations (6) and the kinematic equations (2) and (3) are solved numerically for given terminal poses to yield reference solutions for $\mathbf{x}(\tau)$ and $\mathbf{r}(\tau)$. To assess the accuracy of the shape reconstruction, the difference of position obtained with the approximation from the reference solution is measured with $\varepsilon_\mathrm{r}(\tau) := ||\mathbf{r}(\tau) - \mathbf{r}^{[3]}(\tau)||$. The deviation from the reference orientation is measured with $\varepsilon_\mathrm{x}(\tau) := ||\mathbf{x}(\tau) - \mathbf{x}^{[3]}(\tau)|| \approx ||\log(\exp(-\mathbf{x}(\tau))\exp\mathbf{x}^{[3]}(\tau))||$. The thresholds in the algorithm are set to $\varepsilon_1 = 10^{-3}$ and $\varepsilon_2 = 10^{-5}$.

To demonstrate the method, various relative terminal displacements $\mathbf{H}_{01}$ of the rod's two terminal frames $\mathcal{F}_0$ and $\mathcal{F}_1$ are prescribed. The results for six different terminal displacements are shown in 1. The numerically exact reference solutions are shown in gray, and the shape reconstructed with proposed algorithm is shown in orange. To quantify the approximation accuracy, the orientation error $\varepsilon_\mathrm{r}(\tau)$ and position $\varepsilon_\mathrm{r}(\tau)$ along

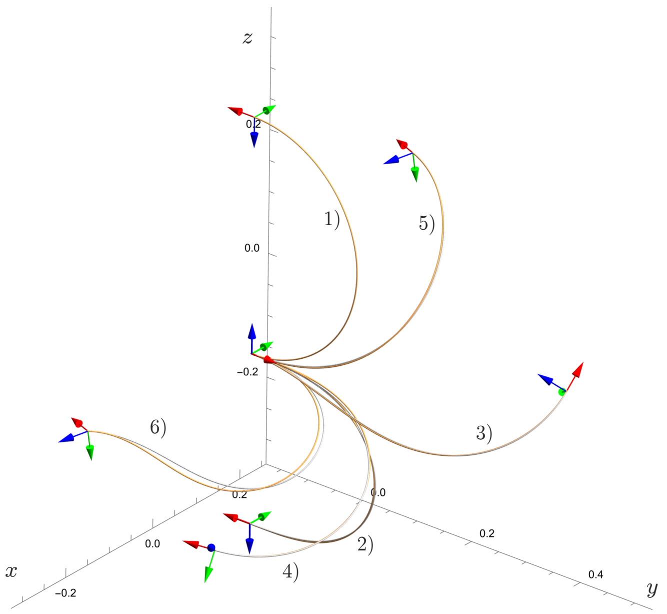

Fig. 1. Shape of the fiberglass element computed with the proposed approximation algorithm for six relative poses of terminal frames $\mathcal{F}_0$ and $\mathcal{F}_1$. The numerically exact solution of the Kirchhoff rod model is shown in gray, the approximation is shown in orange.

the rod are shown in Fig. 2. The convergence of the geometric constraint is shown in Fig. 3. This figure also indicated the number of iterations needed to converge. Fig. 4 shows experimental results for a planar displacement of the terminal ends. The scene was captured with an Intel RealSense D405 camera, and only the 2D-image was used to identify the rod. To improve visibility, the rod was painted with black ink. The central line of the rod was identified with the nearest neighbor algorithm applied to the BW-image. The numerically exact solution of the boundary value problem well fits the approximation computed with the algorithm. Both are in good correspondence with the physical rod. The difference is caused by the parameter uncertainties and the uncertainty of the fixation, which was done manually.

VII. Conclusion and Outlook

Real-time shape reconstruction is crucial for handling and reconfiguration planning of DLO as well as for control of continuum robots. While the modeling using Cosserat and Kirchhoff theory is well established, the efficient solution of the governing boundary value problem remains a key challenge. In this note a computationally efficient algorithm for solving the continuum forward kinematics (CFK) problem of clamped DLO modeled as Kirchhoff rods is introduced. The algorithm yields an explicitly analytic description of the displacement field as a 3rd-order approximation of the exact solution. The accuracy can be improved using 4th-order interpolations as reported in [17], [18]. Another straightforward approach to increase accuracy and to accommodate Accuracy improvements can also be achieved, in particular for very large deformations, by introducing a multi-segment formulation, which allows for varying cross sections and material parameters. Due to its simplicity, the presented method can be

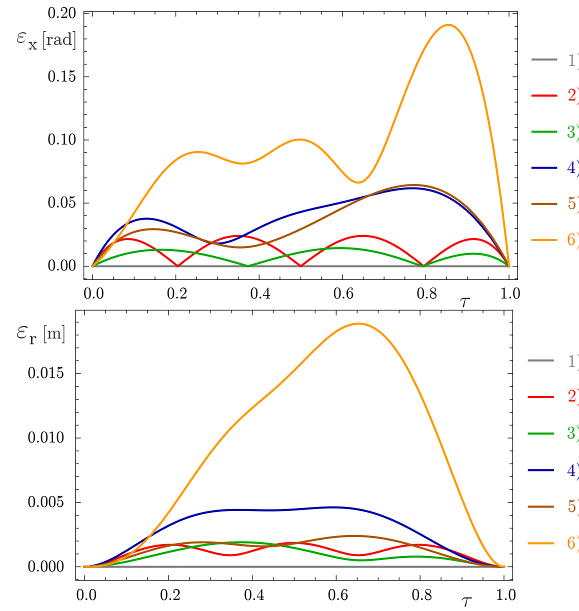

Fig. 2. Approximation errors ε_x and ε_r of the approximations computed with the introduced algorithm for displacements $1) \dots 6)$ accourding to Fig. 1.

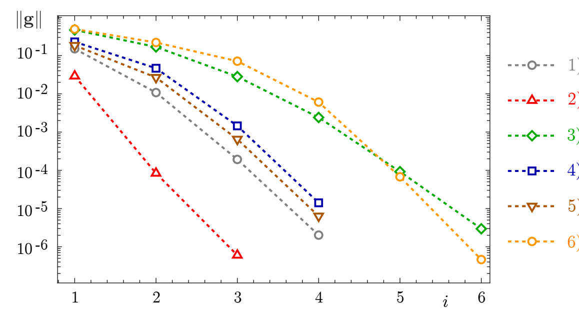

Fig. 3. Evolution of the constraint violation during the iteration process. This also indicates the number of necessary iteration steps.

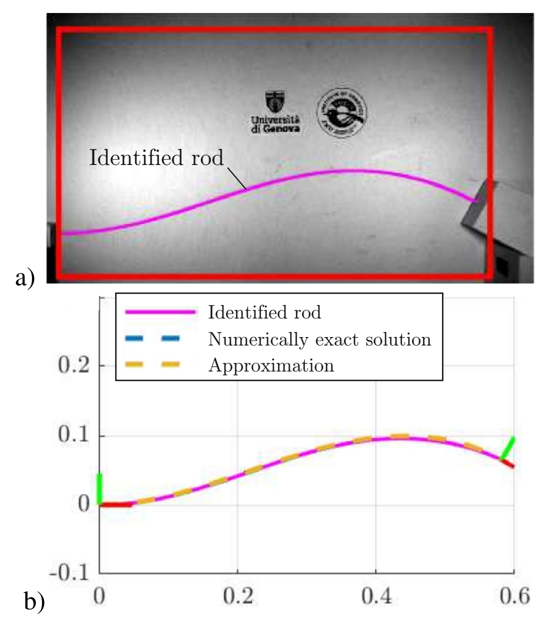

Fig. 4. a) Real experiment with rod identified. b) Superposition of real rod deformation, numerically exact solution, and approximation.

used to provide training data for training of neural networks for shape reconstruction [19], [20].

REFERENCES

[1] J. C. Simo, "A finite strain beam formulation. the three-dimensional dynamic problem. part i," *Computer methods in applied mechanics and engineering*, vol. 49, no. 1, pp. 55–70, 1985.

[2] D. C. Rucker and R. J. Webster III, "Statics and dynamics of continuum robots with general tendon routing and external loading," *IEEE Transactions on Robotics*, vol. 27, no. 6, pp. 1033–1044, 2011.

[3] S. Briot and F. Boyer, "A geometrically exact assumed strain modes approach for the geometrico-and kinemato-static modelings of continuum parallel robots," *IEEE Tran. Rob.*, vol. 39, no. 2, pp. 1527–1543, 2022.

[4] C. Armanini, F. Boyer, A. T. Mathew, C. Duriez, and F. Renda, "Soft robots modeling: A structured overview," *IEEE Transactions on Robotics*, vol. 39, no. 3, pp. 1728–1748, 2023.

[5] D. C. Rucker, B. A. Jones, and R. J. Webster III, "A geometrically exact model for externally loaded concentric-tube continuum robots," *IEEE transactions on robotics*, vol. 26, no. 5, pp. 769–780, 2010.

[6] H. Wang, M. Totaro, and L. Beccai, "Toward perceptive soft robots: Progress and challenges," *Advanced Science*, vol. 5, no. 9, p. 1800541, 2018.

[7] A. L. Orekhov, G. L. H. Johnston, and N. Simaan, "Task and configuration space compliance of continuum robots via lie group and modal shape formulations," pp. 590–597, 2023.

[8] O. Altuzarra, M. Urizar, K. Bilbao, and A. Hernández, "Full forward kinematics of lower-mobility planar parallel continuum robots." *Mathematics (2227-7390)*, vol. 12, no. 22, 2024.

[9] J. Till, V. Aloi, and C. Rucker, "Real-time dynamics of soft and continuum robots based on cosserat rod models," *The International Journal of Robotics Research*, vol. 38, no. 6, pp. 723–746, 2019.

[10] M. Wiese, R. Berthold, M. Wangenheim, and A. Raatz, "Describing and analyzing mechanical contact for continuum robots using a shooting-based cosserat rod implementation," *IEEE Rob. Aut. Let.*, 2023.

[11] A. L. Orekhov and N. Simaan, "Solving Cosserat Rod Models via Collocation and the Magnus Expansion," in *2020 IEEE/RSJ Int. Conf. Int. Rob. Sys. (IROS)*, 2020, pp. 8653–8660.

[12] K. Almaghout, A. Cherubini, and A. Klimchik, "Robotic co-manipulation of deformable linear objects for large deformation tasks," *Robotics and Autonomous Systems*, vol. 175, 2024.

[13] A. Monguzzi, T. Dotti, L. Fattorelli, A. M. Zanchettin, and P. Rocco, "Optimal model-based path planning for the robotic manipulation of deformable linear objects," *Robotics and Computer-Integrated Manufacturing*, vol. 92, p. 102891, 2025.

[14] A. Levin, I. Grinberg, E. Rimon, and A. Shapiro, "Dual arm steering of deformable linear objects in 2-d and 3-d environments using euler's elastica solutions," *arXiv preprint arXiv:2502.07509*, 2025.

[15] R. Murray, Z. Li, and S. Sastry, *A Mathematical Introduction to Robotic Manipulation*. CRC Press, 1994.

[16] A. Müller, "Review of the exponential and Cayley map on SE(3) as relevant for Lie group integration of the generalized Poisson equation and flexible multibody systems," *Proc. Royal Soc. A*, vol. 477.

[17] A. Müller, T. Marauli, and H. Gattringer, "Smooth invariant interpolation on lie groups with prescribed terminal conditions for robot motion planning and modeling of soft robots," in *2024 IEEE/RSJ Int. Conf. Intel. Rob. Sys. (IROS)*. IEEE, 2024, pp. 8442–8448.

[18] A. Müller, "Fourth-Order Accurate Strain-Parameterized Shape Representation of Beam Elements for Modeling Continuum Robots and Robotic Manipulation of Slender Objects," *ASME Journal of Mechanisms and Robotics*, vol. 17, 2024.

[19] M. Yu, K. Lv, H. Zhong, S. Song, and X. Li, "Global model learning for large deformation control of elastic deformable linear objects: An efficient and adaptive approach," *IEEE Tran. Rob.*, vol. 39, no. 1.

[20] Y. Yang, J. A. Stork, and T. Stoyanov, "Learning differentiable dynamics models for shape control of deformable linear objects," *Robotics and Autonomous Systems*, vol. 158, p. 104258, 2022.